*Optica Applicata, Vol. LIV, No. 2, 2024*
DOI: 10.37190/oa240206

# Cantilever-based biaxial FBG inclinometer with low cross-axis sensitivity

NIMALRAJH RAMALINGAM[1], HANGTING YANG[1], KOK-SING LIM[1,*], HARITH AHMAD[1,2]

[1]Photonics Research Centre, University of Malaya,
50603 Kuala Lumpur, Malaysia

[2]Department of Physics, Faculty of Science, University of Malaya,
50603 Kuala Lumpur, Malaysia

[*]Corresponding author: kslim@um.edu.my

This work proposes and demonstrates a biaxial sensing inclinometer based on two FBGs surface-mounted on two separate thin cantilevers with a diminishable cross-axis sensitivity. The measured sensitivities for the inclination angles in the *x*-*z* plane and *y*-*z* plane are 34.87 and 33.49 pm/deg, respectively. To enhance the protection of the delicate FBGs and minimize axis-to-axis cross-sensitivity, the carbon-steel cantilevers are strategically arranged in a perpendicular configuration, resulting in an impressively low cross-sensitivity value of just 0.9275%. This alignment not only offers mechanical shielding but also ensures optimal performance and accuracy for the FBGs.

Keywords: inclinometer, cantilever, cross-sensitivity, fiber Bragg grating.

## 1. Introduction

Tilt sensors or inclinometers have major applications in the engineering and construction industry, especially for bridges and buildings. This is because of their significance in measuring the angular difference of a structure from a set reference plane [1]. The interest in research and development for tilt sensors is rapidly blooming, thus the demands on their measurement precision and technical proficiency are likewise rising [2]. Currently, there are copious types of tilt sensors or inclinometers that are available, such as micro-electro-mechanical systems (MEMS) inclinometers [3-5], pendulum-based tilt sensors [6], single-axis tilt sensors [7], dual-axis tilt sensors [8, 9], and fibre-based tilt sensors [10]. The tilt sensors that are highly reviewed and commercialised are the MEMS inclinometer and fibre-based tilt sensor thanks to their advantageous properties [11]. However, MEMS inclinometers suffer from several drawbacks, including limited bandwidth distance caused by cable attenuation loss, susceptibility to

electromagnetic interference, complicated sensor construction and information-gathering architecture, as well as pricey components [12]. Meanwhile, fibre-based tilt sensors, especially with the development of fibre Bragg grating (FBG) technology, demonstrate more edge when compared to MEMS and interferometer-based inclinometers, considering their excellent resilience to electromagnetic interference and independent temperature capabilities [15]. The FBG sensor also shares the same characteristics of an optical fibre, such as flexible capabilities, easy assembly, small-scale, independent of power supply and rust, *etc*. [16]. FBG-based inclinometer's general performance is based on the variation of the wavelength which is encoded with the information of the change of strain [17] or pressure [18] induced by the structure.

Cross-axis sensitivity in biaxial/multiaxial sensors has always been an undesired property that affects the performance of the measurement [19]. Numerous techniques and designs have been considered to mitigate this issue, such as carefully isolating the sensing elements [20], optimizing mechanical structures [21], or employing calibration procedures [22] to compensate for cross-axis effects. It is an important indicator of efficiency for various applications with different requirements of intricacy and precision [23]. For instance, sensors with cross-axis sensitivity of less than 5% are required for commercial uses, and those less than 0.1% are used for aeronautical applications [24]. The demand for greater precision and dependability of measurements in the fields of construction and engineering is ever-increasing, thus the development of tilt sensors with lower cross-axis sensitivity is a vital area of study.

There have been numerous experimentation reports on FBG-based tilt sensors with distinct techniques but none of the previous works has addressed the importance of cross-axis sensitivity. For example, tilt sensors proposed by ISMAIL *et al*. [1] and HONG *et al*. [25] were devised using the 3D-printed tilt sensors where the fused deposition modelling (FDM) methods using polylactic acid (PLA) materials were adopted to manufacture accurate and linear model using 3D-printers. In their study, ISMAIL *et al*. consider four FBGs with four distinct wavelengths fused to each side of the model making it a biaxial model with an operating range of ±90°, whereas HONG *et al*. analyse the features of the tilt sensor using two FBGs with an operating range of ±75° in the single axial direction. The major disadvantage of using 3D printing, especially using materials like PLA, is that it has lower elasticity modulus and tensile strength compared to other materials such as steel. On the other hand, work done by HE *et al*. [26], BAO *et al*. [27], and AU *et al*. [28], had a different approach, designing a 2D-based model connected to a suspending pendulum with a unique one on each of the model proposed. Although this approach has its advantages such as a high degree of sensitivity and accuracy, the design itself is bulky and heavy for commercial use. Furthermore, GUO *et al*. [29] proposed new advances through which the FBG tilt sensor was conditioned based on a CAM structure that resulted in a large measurement range. Using a cam structure has its drawbacks, for example, this sensor is better suited for detecting static angles due to the cam structure which will oscillate leading to erroneous measurement outcomes. In addition, a simple yet direct modelling approach which is based on

a multifibre bundle that comprises two sensing and two supporting fibres attached to a suspending mass was propounded in [30]. The use of the buoyant method is observed in [31] where two floats are suspended on the surface of the liquid with FBGs attached. Thus under the influence of gravity, the liquid's surface well within the receptacle will establish a new balanced fluid surface plane and alter the liquid's level at various points inside of the receptacle. It is acknowledged that both tilt sensors given had issues, such as sensitivity caused by the enclosed optical fibre into FBG bundle in Li *et al*., which would impede the FBG's mobility, and the use of liquid as a base in a container reported by Chao *et al*., which may confine the measurement range.

In this paper, an FBG-based biaxial inclinometer using a cantilever with diminishable cross-axis sensitivity is proposed and demonstrated. The goal of this study is to fabricate two FBGs which are mounted on the surfaces of the carbon-steel cantilever creating a simple and cost-effective architecture that offers biaxial sensing capability with insignificant cross-axis sensitivity, high accuracy, and linear stability. The retention of low error propagation is another major emphasis of this research.

## 2. Operating principle

Fibre Bragg grating (FBG) is a commonly used optical reflector that is inscribed into a short section of optical fibre that can selectively reflect a narrowband of light while transmitting the rest. By altering the core's refractive index along the fibre, which produces the Bragg wavelength, $\lambda_{\text{Bragg}}$:

$$\lambda_{\text{Bragg}} = 2 n_{\text{eff}} \Lambda \tag{1}$$

where $n_{\text{eff}}$ is the fibre core and $\Lambda$ is the grating period.

The relationship between the Bragg wavelength shift, the change of strain, and the temperature difference, $\Delta T$ and independent from the influence of thermal effect as can be described by linear expressions:

$$\frac{\Delta \lambda_{\text{Bragg}}}{\lambda_{\text{Bragg}}} = (1 - P_{\text{eff}}) \Delta \varepsilon + (\alpha + \xi) \Delta T \tag{2}$$

$$\frac{\Delta \lambda_{\text{Bragg}}}{\lambda_{\text{Bragg}}} = (1 - P_{\text{eff}}) \Delta \varepsilon \tag{3}$$

Figure 1 illustrates the geometry of the cantilever subjects to a tilt angle of $\theta$. One end of the cantilever is fixated at point O, whereas its other end is attached to a metal load at point O′. OA and O′A′ are the vertical lines parallel with the vector of gravity. Suppose OB is the tangent of the cantilever curve at point O, and let O′B′ be an extension from O′ that is parallel with OB. It is safe to deduce that $\angle$A′O′B′ = $\angle$AOB = $\theta$.

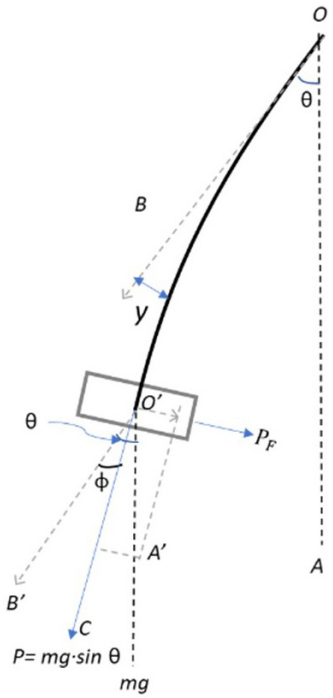


Fig. 1. The geometry of the cantilever with respect to a tilt angle.

When tilted at an angle, $\theta = 90°$, the deflection of the cantilever horizontally can be described as [32]:

$$y = \frac{P}{6EI}(-x^2 + 3xL^2 - 2L^3) \tag{4}$$

where $y$ is the deflection of a horizontal cantilever induced by the load, $P = mg$ which is parallel with the vector of gravity. $P$ is the weight load, $L$ is the length of the cantilever, $E$ is the elasticity of modulus, and $I$ is the area moment of inertia:

$$I = \frac{bh^3}{12} \tag{5}$$

where $b$ is the width of the cantilever and $h$ is the thickness of the cantilever.

Let O′C be a line parallel with the tangent of the cantilever curve at point O′. The deflection angle $\Phi$ at the loaded end of the cantilever (deflection angle from O′B′) given by $\angle$B′O′C, can be estimated from the slope of the cantilever curve, $\Phi = (PL^2)/2EI$. For $\theta < 90°$, the induced load at point O′ of the tilted cantilever also varies with the tilt angle, and it can be described as $P_F = P\sin\theta$.

The radius of curvature can be expressed as:

$$\frac{1}{R} = \frac{y''}{\left(1 + y'^2\right)^{3/2}} \tag{6}$$

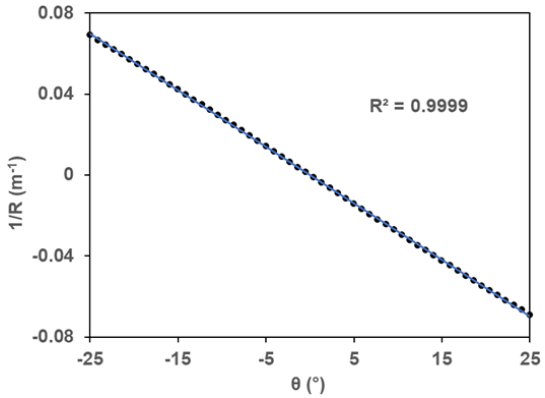


Fig. 2. The relationship between the radius of curvature and tilt angle.

Assuming the FBG is positioned in the middle of the cantilever, $x = L/2$, the relationship between $1/R$ and $\theta$ analysed within the range of –25 to +25°, is as depicted in Fig 2. It can be observed that the relationship between the radius of curvature and the tilt angle can be represented by a linear graph with $R^2 = 0.9999$.

Since the FBG is surface mounted on the cantilever, the induced axial strain, $\varepsilon$ on the FBG by the bending of the cantilever is given by [33]:

$$\varepsilon = z\frac{1}{R} \tag{7}$$

where $z$ denotes height from the unstrained axis (the distance between the fibre axis and the unstrained axis of the cantilever). Based on Eq. (7), the wavelength shifts due to the strain induced by the FBG mounted on the cantilever are linearly proportional to the tilt angle within the range of $-25° < \theta < 25°$, this relationship is shown in the next section.

## 3. Experimental setup

The operating principle of the proposed inclinometer is based on the bending of the cantilever that induces tensile/compressive strains on the FBG that is mounted on the surface of the cantilever. The proposed inclinometer mainly comprises carbon steel spring plates that serve as the substrates and metal loads as illustrated in Fig. 3(a). The use of carbon steel plates offers the advantage of limiting the motion/bending of the FBG in the specific plane and preventing the twisting and torsion of the entire structure which can lead to cross-axis sensitivity between the two axes. Two 5 mm grating, denoted as $FBG_x$ and $FBG_y$ with the Bragg wavelengths of 1543.9 and 1553.6 nm were employed for sensing two orthogonal axes and an additional $FBG_T$ with a wavelength of 1556.2 nm was for temperature compensation. Both $FBG_x$ and $FBG_y$ were securely affixed to the surfaces of carbon steel plates measuring 40 × 3 × 0.2 mm in dimension utilizing epoxy as the adhesive.

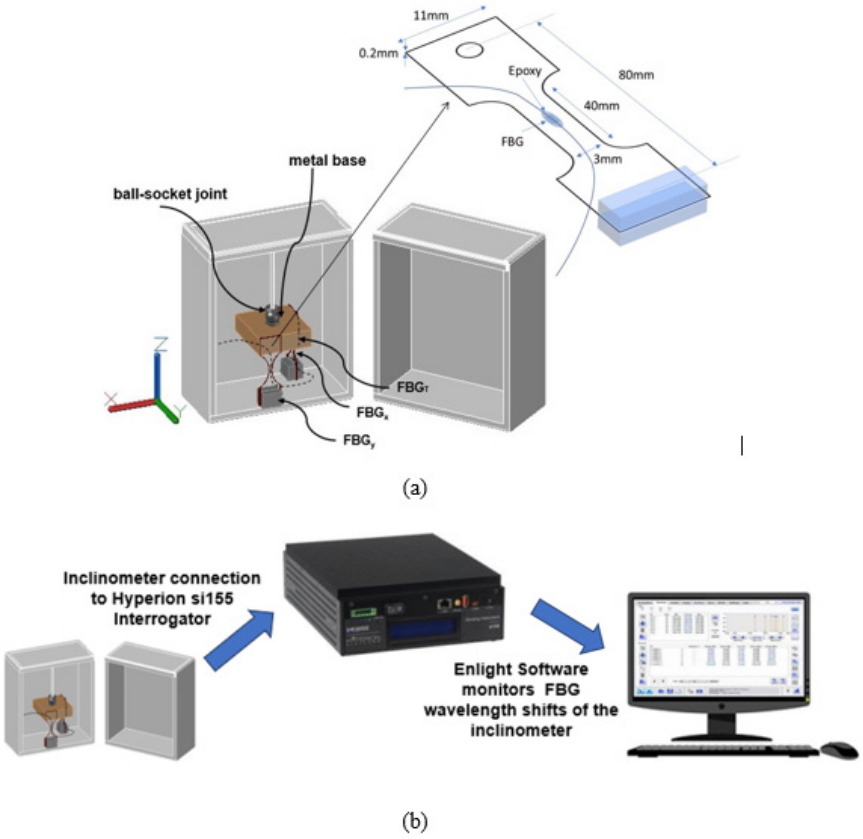


Fig. 3. (a) Schematic illustration of the proposed inclinometer, and (b) experimental setup.

In addition to the fixation, the epoxy, and the carbon steel plates also provide extra protection to the fragile FBGs. The carbon steel plates with the respective FBG attached were fixated on a rectangular metal block and aligned perpendicular to each other. This ensures that both FBGs are only sensitive to the inclination in their respective tilt plane (*x*-*z* plane and *y*-*z* plane). A ball-socket joint is intended for the adjustment of the initial angles of the inclinometer so that both grating axes of FBGs are perfectly parallel to gravity. In addition to the two FBGs, a third FBG, $FBG_T$ is incorporated into the FBG array for temperature compensation.

After that, the proposed inclinometer is characterized between the range of –25° to 25° with an increment step of 5° for both planes. For the characterization test, the FBG array was connected to an FBG interrogator (Micron Optics Hyperion si155) for spectral analysis and data acquisition as shown in Fig. 3(b). A commercial tiltmeter with a measurement range of 0° to 90° and an accuracy of 0.1° is used as the reference. The commercial tiltmeter was mounted on the surface of the rectangular metal block and the inclinometer was tilted manually until the desired angle (based on the reading of the tiltmeter) was achieved.

## 4. Results and discussion

As highlighted before, the proposed model with two distinct wavelengths, $FBG_x$ and $FBG_y$ was evaluated between –25° to 25° with an incremental step of 5° for each tilt plane. The interception wavelength at 0° for $FBG_x$ in the *x*-*z* plane and $FBG_y$ in the *y*-*z* plane was measured to be 1543.9 and 1553.6 nm, respectively.

Angular sensitivity, cross-axis sensitivity, resolution, and accuracy are the key components that were investigated during the characterization test. To obtain the average angular sensitivity and the perpendicular angular sensitivities, one of the axes was made constant, say $\theta_x = –25°$ while the other angle, $\theta_y$ was varied from –25° to 25° at the incremental step of 5°. The same test cycle was repeated for different angles in $\theta_x = –20°, –15°, ..., 25°$ while $\theta_y$ was made constant and the wavelength shift was recorded. Figure 4(a) shows some example reflection spectra for varying $\theta_x$ and fixed $\theta_y$. $FBG_x$ redshifts but $FBG_y$ is insensitive to varying $\theta_x$. The relationship between the wavelength shifts of $FBG_x$ and $FBG_y$ with $\theta_x$ is presented in Fig. 4(b). $FBG_x$ has shown an angular sensitivity of $k_{xx} = 34.87$ pm/deg with a proportional linearity of

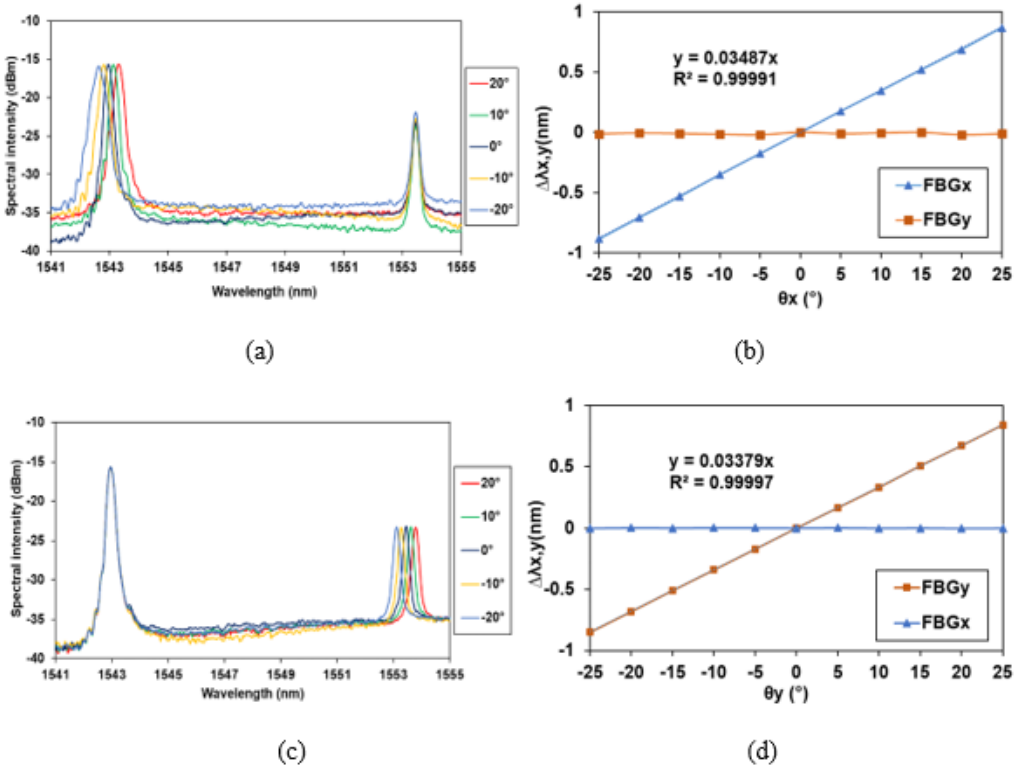


Fig. 4. (a) Spectral responses of $FBG_x$ and $FBG_y$ for varying $\theta_x$ and fixed $\theta_y = 0°$. (b) The plot of wavelength shifts of $FBG_x$ and $FBG_y$ against varying $\theta_x$ and fixed $\theta_y = 0°$. (c) Spectral responses of $FBG_x$ and $FBG_y$ for varying $\theta_y$ and fixed $\theta_x = 0°$. (d) The plot of wavelength shifts of $FBG_x$ and $FBG_y$ against varying $\theta_y$ and fixed $\theta_x = 0°$.

$R^2 = 0.99991$. On the other hand, the spectral responses of $FBG_x$ and $FBG_y$ with varying $\theta_y$ and fixed $\theta_x$ are presented in Fig. 4(c). $FBG_y$ redshifts but $FBG_x$ is idle with increasing $\theta_y$. $FBG_y$ based on Fig. 4(d) has shown a similar angular sensitivity of $k_{yy} = 33.79$ pm/deg with $R^2 = 0.99997$.

### 4.1. Cross-axis compensation

Generally, in a biaxial inclinometer, when one of the axes experiences inclinations, it will cause the perpendicular axis to undesired distortion on the wavelength shift which makes it vulnerable to higher cross-axis sensitivity. Thus, The relationships between the wavelength shifts and tilt angles of $FBG_x$ and $FBG_y$ can be described by the linear expressions:

$$\Delta\lambda_x = k_{xx}\theta_x + k_{xy}\theta_y + \gamma_x\Delta T \tag{8}$$

$$\Delta\lambda_y = k_{yy}\theta_y + k_{yx}\theta_x + \gamma_y\Delta T \tag{9}$$

where $k_{xx}$ and $k_{yy}$ are the angular sensitivities of the $FBG_x$ and $FBG_y$, respectively, while $k_{xy}$ and $k_{yx}$ are the perpendicular axis sensitivities.

The impact of the cross-axis sensitivity on the measurement accuracy can be evaluated based on the following normalized cross-axis sensitivities:

$$\frac{k_{xy}}{k_{xx}} = x - z\text{-axis} \tag{10}$$

$$\frac{k_{yx}}{k_{yy}} = y - z\text{-axis} \tag{11}$$

From the characterisation results in Fig. 4, the perpendicular axis sensitivities of $FBG_x$ and $FBG_y$ are measured to be $k_{xy} = 2.6992 \times 10^{-2}$ pm/° and $k_{yx} = 3.6198 \times 10^{-2}$ pm/°.

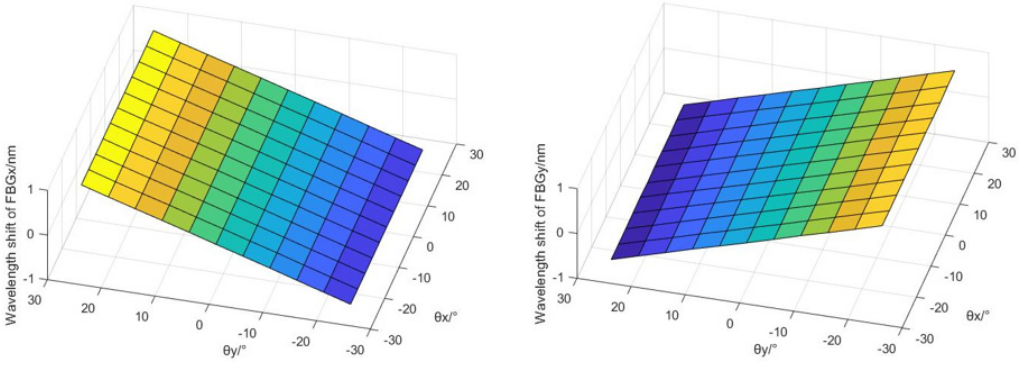


(a) (b)

Fig. 5. (a) The visualisation of cross-axis sensitivity on $FBG_x$. (b) The visualisation of cross-axis sensitivity on FBG.

The normalized cross-axis sensitivities $k_{xy}/k_{xx}$ and $k_{yx}/k_{yy}$ for the *x*-*z* axis and *y*-*z* axis was calculated to be 0.774% and 1.081%, respectively, which average 0.9275%. Figure 5 illustrates the visualisation of the cross-axis sensitivities of $FBG_x$ and $FBG_y$ during inclination from –25° to 25°.

In Fig. 5, the graph illustrates the minimal cross-axis sensitivity of the proposed model, showcasing its compatibility with the values obtained through Eq. (10) and Eq. (11) for normalized cross-axis sensitivities. Specifically, when tilted along the $\theta_y$ and $\theta_x$ axes, the disparity in wavelength shifts is evident. However, the impact of these shifts on the cross-axis is negligible, indicating a diminutive effect. The observed low interaction between the two axes enables us to disregard any potential cross-axis effects. Consequently, this characteristic enhances the stability and reliability of the proposed model.

## 4.2. Temperature compensation

Figure 6(a) presents the spectral response of the $FBG_x$, $FBG_y$, and $FBG_T$ to temperatures in the range of 24–44°C. All Bragg wavelengths experience red shifting with

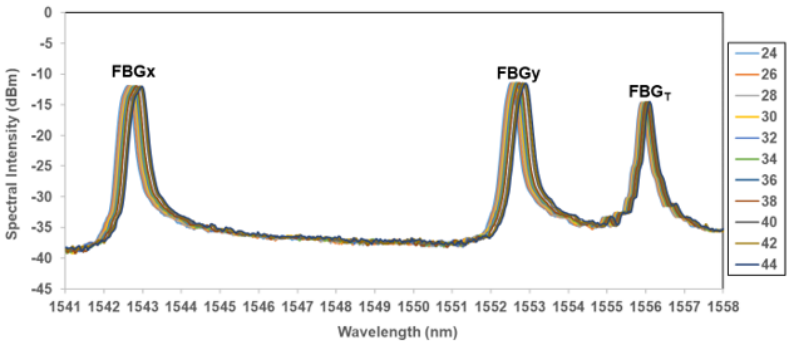


(a)

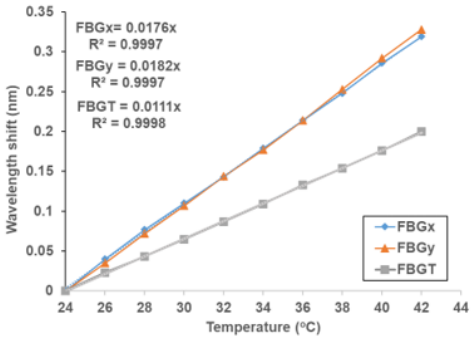


(b)

Fig. 6. (a) Spectral response of the FBGs to temperature change. (b) Linear relationship between wavelength shifts and temperature.

increasing temperature. The measured temperature sensitivities of $FBG_x$, $FBG_y$, and $FBG_T$ are $\gamma_x = 0.0176$ nm/°C, $\gamma_y = 0.0182$ nm/°C and $\gamma_T = 0.0111$ nm/°C, respectively. The higher temperature sensitivities of both $FBG_x$ and $FBG_y$ can be attributed to the carbon steel plates that have a larger TEC.

Based on the acquired experimental data and equation obtained from Eqs. (8) and (9). the general relationship between the wavelength shift, tilt angles, and temperature change for $FBG_T$, $FBG_x$, and $FBG_y$ with negligible cross-axis sensitivity can be expressed as

$$\Delta\lambda_T = \gamma_T \Delta T \tag{12}$$

$$\Delta\lambda_x = \gamma_x \Delta T + k_{xx}\theta_x \tag{13}$$

$$\Delta\lambda_y = \gamma_y \Delta T + k_{yy}\theta_y \tag{14}$$

Thus, by substituting (12) into (13) and (14), the following expressions are attained.

$$\theta_x = \frac{\Delta\lambda_x}{k_{xx}} - \frac{\Delta\lambda_T}{\gamma_T}\gamma_x \tag{15}$$

$$\theta_y = \frac{\Delta\lambda_y}{k_{yy}} - \frac{\Delta\lambda_T}{\gamma_T}\gamma_y \tag{16}$$

where $\gamma_x$, $\gamma_y$ and $\gamma_T$ are the temperature coefficients for $FBG_x$, $FBG_y$, and $FBG_T$, $k_{xx}$ and $k_{yy}$ is the angular coefficients and $\Delta T$ is the temperature change.

Figure 7 compares the results of the measurement from the experiment and estimation using Eqs. (15) and (16). The estimated angles for $\theta_x$ and $\theta_y$ coincide with the experimental measurement very well. This is due to the minimisation of the cross-axis sensitivity that reflects on the stability and accuracy of the proposed inclinometer.

Assuming $\Delta T = 0$, the accuracy of the estimation based on Eqs. (15) and (16) is assessed using mean absolute error (MAE):

$$\text{MAE} = \frac{1}{n}\sum \left|\text{Experiment} - \text{Estimation}\right| \tag{17}$$

The mean absolute error (MAE) for $\theta_x$ and $\theta_y$ is observed to be 0.1059° and 0.1299°, respectively. These MAE values serve as indicators of the overall accuracy of the proposed inclinometer. To further evaluate the relative accuracy of this work, the obtained MAE was utilized to calculate the mean relative absolute error (MRAE):

$$\text{MRAE} = \frac{1}{n}\sum \left|\frac{\text{Experiment} - \text{Estimation}}{\text{Experiment}}\right| \tag{18}$$

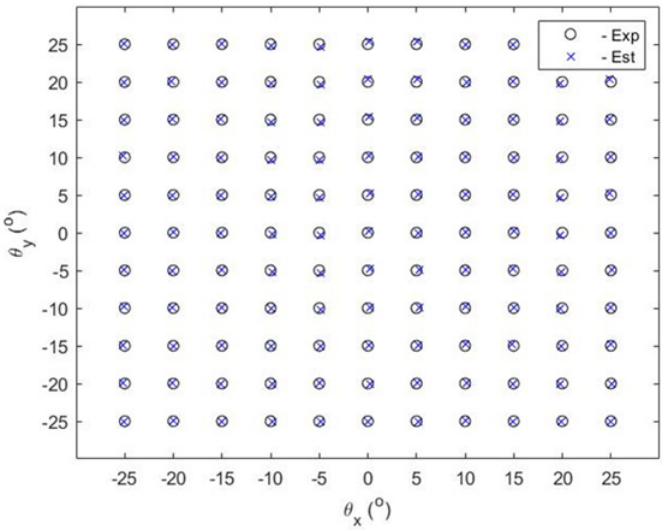


Fig. 7. Comparison graph between experimental data and estimated data for $\theta_x$ and $\theta_y$.

The MRAE of $\theta_x$ and $\theta_y$ is calculated to be 0.1628% and 0.2303% (the data for 0° accepted values are excluded). These MRAE values provide an assessment of the relative accuracy of the model concerning the respective axes and a low MRAE percentage suggests that the inclinometer provides precise and reliable measurements with minimal relative error. Figure 7 and the calculated mean absolute error (MAE) collectively demonstrate that the inclinometer exhibits a high level of precision. These findings align with the characteristics typically associated with various types of inclinometers. Based on the wavelength resolution of the FBG interrogator which is 1 pm in value and the obtained average sensitivity of both FBGs ($k_{xx}$ = 34.87 pm/° and $k_{yy}$ = 33.79 pm/°), the equivalent resolutions for $FBG_x$ and $FBG_y$ are estimated to be ±0.0287° and ±0.0299°, respectively. The proposed accuracy and resolution allow for precise measurements and is suitable for many applications where high accuracy is required. However, the suitability of this resolution depends on the specific application and the level of precision needed.

The Table presents a comparison of the performance of various FBG-based tilt sensors/inclinometers. While studies by Bao *et al*. and Guo *et al*. demonstrate higher sensitivities and resolutions compared to the proposed model, the proposed sensor excels in terms of accuracy. The cantilever-based configuration contributes to the proposed sensor's ability to achieve eminent accuracy and low MRAE which are 0.1628% and 0.2303% for $\theta_x$ and $\theta_y$. The structural design minimizes the cross-sensitivity which is an undesired parasitic effect. This ensures that the measured tilt values closely align with the true tilt angles. On the other hand, Li *et al*. and Ismail *et al*. showed an operating range greater than that of this study, yet the proposed sensor exhibits higher sen-

T a b l e. Attributes of different FBG-based tilt sensors.

| | Range [°] | Sensitivity [pm/°] | Accuracy [°] | Resolution [°] | Cross-axis sensitivity [%] |
|---|---|---|---|---|---|
| HE *et al*. (2009) | –12 to +12 | 192 | 0.1 | 0.005 | – |
| BAO *et al*. (2010) | –40 to +40 | *x*-axis: 96, 80<br>*y*-axis: 79, 93.6 | 0.2 | 0.013 | – |
| AU *et al*. (2011) | –35 to +35 | 39.5 | 0.051 | 0.013 | – |
| CHAO *et al*. (2018) | –5 to +5 | *x*-axis: 132<br>*y*-axis: 128 | – | – | – |
| LI *et al*. (2020) | –50 to +50 | 4.5 | – | – | – |
| GUO *et al*. (2020) | –90 to +90 | 46.7 | 1.516 | 0.003 | – |
| ISMAIL *et al*. (2021) | –90 to +90 | 10 | – | – | – |
| This work | –25 to +25 | *x*-axis: 34.87<br>*y*-axis: 33.79 | $\theta_x$: 0.1059<br>$\theta_y$: 0.1299 | $\theta_x$: 0.0287<br>$\theta_y$: 0.0299 | 0.9275 |

sitivity due to the consideration made in sensor design, and the proposed inclinometer is optimized to achieve accurate measurements within its specified range. Notably, the proposed sensor offers a comprehensive range of performance capabilities. While discussions in various studies have primarily centered around the fundamental sensitivities of the orthogonal axes, the effects of these sensitivities are often neglected due to their lower magnitudes compared to the main axes. However, a thorough exploration of cross-axis sensitivity analysis between these axes is frequently overlooked. This oversight is particularly significant for the prospective industrial applications of these sensors. In contrast, the sensor proposed in this study is designed with low cross-axis sensitivity, a critical specification for biaxial sensors. This feature is particularly essential for ensuring reliability and durability in practical applications.

## 5. Conclusion

A cantilever-based inclinometer using two FBGs for biaxial sensing (*x*-*z* and *y*-*z* axis) with minimised cross-axis sensitivity between both axes was fabricated and characterised. When the inclinometer is tilted, the loaded cantilevers are bent due to the gravitational effect, thus inducing axial strain on the FBGs mounted to the surface of the cantilever. As a result, the Bragg wavelengths are shifted by the tilt angle in the tilt plane. The measured sensitivities for $FBG_x$ and $FBG_y$ are 34.87 and 33.79 pm/°, respectively, with a minimised cross-axis sensitivity of 0.9275%. The proposed inclinometer also offers high accuracy of 0.1059° and 0.1299 over the range of ±25° for both tilt planes. The proposed inclinometer possesses diminishable cross-sensitivity, and the mean relative absolute error (MRAE) for $FBG_x$ and $FBG_y$ is calculated to be 0.1628% and 0.2303%. Overall, a straightforward, stable, cost-effective, and simple inclinometer was fabricated with excellent characteristics such as inclined sensitivities, diminutive cross-axis sensitivity, low MRAE, low angular error, high accuracy,

and a good resolution. This inclinometer is suitable for structural health monitoring and ground movement monitoring.

**Acknowledgment**
The work is supported by Technology Development Fund 1 (TED1), MOSTI (TDF06221580, MOSTI003 -2023TED1), and UM Matching Grant (MG029-2022).

## References

[1] Ismail N., Sharbirin A.S., Sa'ad M., Zaini M.K.A., Ismail M.F., Brambilla G., Rahman B.M.A., Grattan K.T.V., Ahmad H., *Novel 3D-printed biaxial tilt sensor based on fibre Bragg grating sensing approach*, Sensors and Actuators A: Physical **330**, 2021: 112864. https://doi.org/10.1016/j.sna.2021.112864

[2] Xu Y., Jiang Q., Yang K., Zhou J., Guo Q., *A novel ultra-high-resolution inclination sensor based on diamagnetic levitation*, Sensors and Actuators A: Physical **343**, 2022: 113686. https://doi.org/10.1016/j.sna.2022.113686

[3] Bahri R., Boucetta R., Bel Hadj Ali Naoui S., *An innovative tilt sensor based on terrestrial gravity and ultrasonic wave's diffraction for mobile robots*, [In] *2018 15th International Multi-Conference on Systems, Signals & Devices (SSD)*, Yasmine Hammamet, Tunisia, 2018, pp. 821-826. https://doi.org/10.1109/SSD.2018.8570475

[4] Tang L.J., Zhang K., Chen S., Zhang G.J., Liu G.W., *MEMS inclinometer based on a novel piezoresistor structure*, Microelectronics Journal **40**(1), 2009: 78-82. https://doi.org/10.1016/J.MEJO.2008.06.080

[5] Segalini A., Chiapponi L., Pastarini B., Carini C., *Automated Inclinometer Monitoring Based on Micro Electro-Mechanical System Technology: Applications and Verification*, [In] *Landslide Science for a Safer Geoenvironment*, [Eds.] Sassa K., Canuti P., Yin Y., Springer, Cham, 2014. https://doi.org/10.1007/978-3-319-05050-8_92

[6] Han Q., Chen C., *Research on tilt sensor technology*, [In] *2008 IEEE International Symposium on Knowledge Acquisition and Modeling Workshop*, Wuhan, China, 2008: 786-789. https://doi.org/10.1109/KAMW.2008.4810608

[7] Yuliza E., Habil H., Salam R.A., Munir M.M., Abdullah M., Khairurrijal, *Development of a simple single-axis motion table system for testing tilt sensors*, Procedia Engineering **170**, 2017: 378-383. https://doi.org/10.1016/J.PROENG.2017.03.061

[8] Su W., Fu J., *The study of variable sensitivity in dual-axis tilt sensor*, Procedia Engineering **29**, 2012: 2605-2609. https://doi.org/10.1016/J.PROENG.2012.01.359

[9] Ha Tran Thi Thuy, Tiep Dang Dinh, Tuan Vu Quoc, Thinh Pham Quoc, Masahiro Aoyagi, My Bui Ngoc, Van Thanh Dau, Tung Thanh Bui, *A robust two-axis tilt angle sensor based on air/liquid two-phase dielectric capacitive sensing structure*, IETE Journal of Research **66**(5), 2020: 685-696. https://doi.org/10.1080/03772063.2018.1518732

[10] Zheng D., Cai Z., Floris I., Madrigal J., Pan W., Zou X., Sales S., *Temperature-insensitive optical tilt sensor based on a single eccentric-core fiber Bragg grating*, Optics Letters **44**(22), 2019: 5570-5573. https://doi.org/10.1364/OL.44.005570

[11] Łuczak S., Ekwińska M., *Electric-contact tilt sensors: A review*, Sensors **21**(4), 2021: 1097. https://doi.org/10.3390/S21041097

[12] Lim K.-S., Ong Z.-C., Lee Y.-S., Bin Zaini M.K.A., Ahmad H., *Pseudohigh-resolution spectral interrogation scheme for small signals from FBG sensors*, IEEE Transactions on Instrumentation and Measurement **68**(8), 2019: 2964-2970. https://doi.org/10.1109/TIM.2018.2871279

[13] SHARBIRIN A.S., ZAINI M.K.A., BRAMBILLA G., RAHMAN B.M.A., GRATTAN K.T.V., ISMAIL M.F., AHMAD H., *3D-printed tilt sensor based on an embedded two-mode fiber interferometer*, IEEE Sensors Journal **21**(6), 2021: 7565-7571. https://doi.org/10.1109/JSEN.2021.3050756

[14] LIAO H., LU P., FU X., JIANG X., NI W., LIU D., ZHANG J., *Sensitivity amplification of fiber-optic in-line Mach–Zehnder Interferometer sensors with modified Vernier-effect*, Optics Express **25**(22), 2017: 26898-26909. https://doi.org/10.1364/OE.25.026898

[15] MIHAILOV S.J., *Fiber Bragg grating sensors for harsh environments*, Sensors **12**(2), 2012: 1898-1918. https://doi.org/10.3390/S120201898

[16] PAN J., WANG L., HOU W., *Design and investigation of a high-sensitivity tilt sensor based on FBG*, Photonic Sensors **13**, 2023: 230228. https://doi.org/10.1007/S13320-022-0671-8

[17] VINNARASI K., SUNDARAVADIVELU S., *Strain measurement using fiber Bragg grating sensor for crack detection*, International Journal of Advanced Engineering Research and Science **4**(3), 2017: 219-223. https://doi.org/10.22161/IJAERS.4.3.35

[18] PACHAVA V.R., KAMINENI S., MADHUVARASU S.S., PUTHA K., MAMIDI V.R., *FBG-based high-sensitive pressure sensor and its low-cost interrogation system with enhanced resolution*, Photonic Sensors **5**, 2015: 321-329. https://doi.org/10.1007/S13320-015-0259-7

[19] HILLER T., BLOCHER L., VUJADINOVIC M., PENTEK Z., BUHMANN A., ROTH, H., *Analysis and compensation of cross-axis sensitivity in low-cost MEMS inertial sensors*, [In] *2021 IEEE International Symposium on Inertial Sensors and Systems (INERTIAL)*, Kailua-Kona, HI, USA, 2021: 1-4. https://doi.org/10.1109/INERTIAL51137.2021.9430454

[20] NGUYEN M.N., NGUYEN L.Q., CHU H.M., VU H.N., *A two degrees of freedom comb capacitive-type accelerometer with low cross-axis sensitivity*, Journal of Mechanical Engineering and Sciences **13**(3), 2019: 5334-5346. https://doi.org/10.15282/jmes.13.3.2019.09.0435

[21] DIN H., IQBAL F., LEE B., *Design approach for reducing cross-axis sensitivity in a single-drive multi-axis MEMS gyroscope*, Micromachines **12**(8), 2021: 902. https://doi.org/10.3390/mi12080902

[22] JATININGRUM D., DE VISSER C., VAN PAASSEN M.M., CHU Q.P., MULDER M., *Investigating cross-axis sensitivity and misalignment in an angular accelerometer measurement unit*, AIAA Guidance, Navigation, and Control Conference, Grapevine, Texas, 2017. https://doi.org/10.2514/6.2017-1905

[23] HSU Y.-W., CHEN J.-Y., CHIEN H.-T., CHEN S., LIN S.-T., LIAO L.-P., *New capacitive low-g triaxial accelerometer with low cross-axis sensitivity*, Journal of Micromechanics and Microengineering **20**, 2010: 055019. https://doi.org/10.1088/0960-1317/20/5/055019

[24] MOHAMMED Z., GILL W.A., RASRAS M., *Double-comb-finger design to eliminate cross-axis sensitivity in a dual-axis accelerometer*, IEEE Sensors Letters **1**(5), 2017: 2501004. https://doi.org/10.1109/LSENS.2017.2756108

[25] HONG C.Y., ZHANG Y.F., LU Z., YIN Z.Y., *A FBG tilt sensor fabricated using 3D printing technique for monitoring ground movement*, IEEE Sensors Journal **19**(15), 2019: 6392-6399. https://doi.org/10.1109/JSEN.2019.2908873

[26] HE S.L., DONG X.Y., NI K., JIN Y.X., CHAN C.C., SHUM P., *Temperature-insensitive 2-D tilt sensor with three fiber Bragg gratings*, Measurement Science and Technology **21**, 2010: 025203. https://doi.org/10.1088/0957-0233/21/2/025203

[27] BAO H.L., DONG X.Y., ZHAO C.L., SHAO L.-Y., CHAN C.C., SHUM P., *Temperature-insensitive FBG tilt sensor with a large measurement range*, Optics Communications **283**(6), 2010: 968-970. https://doi.org/10.1016/J.OPTCOM.2009.11.014

[28] AU H.Y., KHIJWANIA S.K., FU H.Y., CHUNG W.H., TAM H.Y., *Temperature-insensitive fiber Bragg grating based tilt sensor with large dynamic range*, Journal of Lightwave Technology **29**(11), 2011: 1714-1720. https://doi.org/10.1109/JLT.2011.2132695

[29] GUO Y.X., LI C., ZHOU X.L., JIANG L., LIU H.H., *Wide-range fiber Bragg grating tilt sensor based on a cam structure*, IEEE Sensors Journal **20**(9), 2020: 4740-4748. https://doi.org/10.1109/JSEN.2020.2967088

[30] LI K., ZHAO Y.H., LI Y.Q., LIU G.Y., LI J., *Fiber Bragg grating biaxial tilt sensor using one optical fiber*, Optik **218**, 2020: 164973. https://doi.org/10.1016/J.IJLEO.2020.164973

[31] Chao C.-R., Liang W.-L., Liang T.-C., *Design and testing of a 2D optical fiber sensor for building tilt monitoring based on fiber Bragg gratings*, Applied System Innovation **1**(1), 2018: 2. https://doi.org/10.3390/ASI1010002

[32] Beer F., Johnston E.R. Jr., DeWolf J., Ma J., *Mechanics of Materials*, 7th Ed., Chapter 9, McGraw -Hill Education, 2014.

[33] Gengnagel C., Lafuente Hernández E., Bäumer R., *Natural-fibre-reinforced plastics in actively bent structures*, Proceedings of the Institution of Civil Engineers - Construction Materials **166**(6), 2013: 365-377. https://doi.org/10.1680/COMA.12.00026

*Received September 21, 2023*
*in revised form January 16, 2024*